Glassy swirls of active dumbbells

Rituparno Mandal,[1,*] Pranab Jyoti Bhuyan,[1,†] Pinaki Chaudhuri,[2,‡] Madan Rao,[3,§] and Chandan Dasgupta[1,¶]

[1] *Centre for Condensed Matter Theory, Department of Physics, Indian Institute of Science, Bangalore 560012, India*
[2] *The Institute of Mathematical Sciences, Chennai 600113, India*
[3] *Simons Centre for the Study of Living Machines, National Centre for Biological Sciences (TIFR), Bangalore 560065, India*

The dynamics of a dense binary mixture of soft dumbbells, each subject to an active propulsion force and thermal fluctuations, shows a sudden arrest, first to a translational then to a rotational glass, as one reduces temperature T or the self-propulsion force f. Is the temperature-induced glass different from the activity-induced glass ? To address this question, we monitor the dynamics along an iso-relaxation-time contour in the $(T-f)$ plane. We find dramatic differences both in the fragility and in the nature of dynamical heterogeneity which characterise the onset of glass formation - the activity-induced glass exhibits large swirls or vortices, whose scale is set by activity, and appears to diverge as one approaches the glass transition. This large collective swirling movement should have implications for collective cell migration in epithelial layers.

PACS numbers: 61.20.Ja, 64.70.D-, 64.70.P-

arXiv:1703.05484v1 [cond-mat.soft] 16 Mar 2017

Assemblies of self-propelled objects jam at high densities [1–4] and low temperatures [5]. On approaching dynamical arrest from the fluid side, these dense active assemblies are seen to exhibit typical glassy dynamics, with activity manifesting simply as an *effective temperature* [5, 6]. Likewise, starting from the jammed state, activity is seen to prematurely *fluidize* the system at a reduced (enhanced) transition temperature (volume fraction) [1–5]. On the face of it, it might appear that an active glass behaves very similar to a conventional one, albeit with a different effective temperature or density [1, 6]. In this paper, we provide evidence to the contrary - we show that an active glass exhibits distinctive dynamical features on account of their local driving.

To address this, we study dense assemblies of generic oriented nonspherical self-propelled objects [7–12], which are free to explore both translational and orientational degrees of freedom. Living realisations include reconstituted layer of confluent epithelial cells [13], where cell shape anisotropy plays a crucial role in the jamming-unjamming transition [14], and jammed biofilms formed by a dense collection of rod-shaped bacteria. Likewise, shaken non-spherical grains at high packing densities constitute non-living examples [15].

We perform Brownian dynamics simulations of a dense binary assembly of dumbbells [16–19] in 2-dimensions (see Fig. 1(a) and *Supplementary Information* [20] for details); the 50:50 mixture of A and B type dumbbells ensures amorphous steady state structures. This assembly, subject to a temperature bath T, is made active by driving each dumbbell with a body-fixed propulsion force f along the long axis of each dumbbell, and is characterized by a Peclet number $Pe \equiv f\sigma_{AA}/k_BT$, measuring the relative strength of activity with respect to temperature [7, 12]. The phase diagram Fig. 1(b) shows a jammed state upon reducing either temperature or self-propulsion force. Our main result is that the dynamical signatures of an active glass are fundamentally different from a conventional glass - (i) activity makes the glass less fragile (Fig. 1(c)), and (ii) the nature of dynamical heterogeneity in an active glass is very unique and exhibits large scale swirls and vortices (Fig. 2(a)), whose size increases and appears to diverge as one approaches the arrested state (Fig. 3(b)) by reducing the self propulsion force f. We understand these length scales from a continuum hydrodynamic theory of active dumbbells. These large scale swirls are the sluggish imprints of the collective turbulent motion observed in an active fluid of anisotropic particles [9, 10, 21].

To identify the onset of translational and rotational glassy behaviour in the $(T-f)$ plane, we monitor the mean-square-displacement (MSD), $\langle \Delta\mathbf{r}(t)^2\rangle = \langle \frac{1}{N}\sum_i \langle |\mathbf{r}_i(t_0+t)-\mathbf{r}_i(t_0)|^2\rangle$, where $\mathbf{r_i}$ is the center-of-mass of the i^{th}-dumbbell; the orientation correlation function $C_2(t) = \frac{1}{N}\sum_i \langle P_2\left[\mathbf{n}_i(t_0)\cdot\mathbf{n}_i(t_0+t)\right]\rangle$ [17, 18], where P_2 is the 2^{nd}-order Legendre polynomial and $\mathbf{n}_i$ is the unit vector along the long axis of the i^{th} dumbbell; and the overlap function $Q(t) = \langle \frac{1}{N}\sum_i w(|\mathbf{r}_i(t_0) - \mathbf{r}_i(t_0+t)|)\rangle$, where $w(r) = 1$ if r $\leq$ a and 0 if r $>$ a, with a=0.3 [22]. Here, $\langle\cdots\rangle$ denotes an average over time origins t_0 and trajectories and N is the number of dumbbells.

Note the following - (i) the dumbbells are subject to thermal noise and active propulsion; (ii) there is no explicit activity decorrelation time, orientational decorrelation occurs because of collisions and thermal fluctuations; and (iii) there is no imposed orientational alignment, any kind of orientation correlation appears entirely due to packing and collisions.

Starting from the liquid phase at high temperature T and activity f, we reduce either T or f. The MSD (*Supplementary Figure S1* [20]) shows cage diffusion, with a distinct intermediate plateau and a reduced late time diffusion coefficient, characteristic of the approach to a glass, as the temperature or activity is reduced. The boundary to the glassy phase is associated with the vanishing of the late time diffusion coefficient. This is ac-

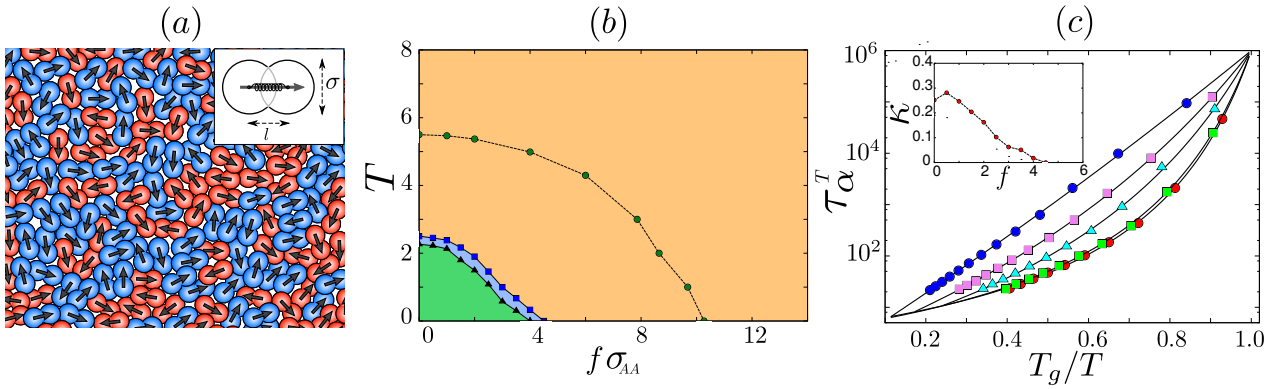

FIG. 1. (color online) (a) Schematic of a dense binary assembly of self-propelled dumbbells of A (blue) or B (red) type. Inset shows structural details of each dumbbell - two identical soft Lennard-Jones spheres of diameter σ connected through a simple spring of spring constant k and rest length l. The body-fixed self-propulsion force f (arrow) is along the long axis of each dumbbell. (b) Phase diagram in $(T-f)$ plane shows a liquid (L, in brown), translational glass (TG, in blue) and translational-rotational glass (TRG, in green) with phase boundaries determined from VFT fits. The dashed line represents the iso-relaxation time ($\tau_\alpha^T = 102.85$) line, along which the dynamics is probed at points marked in green. (c) Variation of translational relaxation times τ_α^T versus scaled temperature (T/T_g) with changing active force : $f = 0$ (red), $f = 1$ (green), $f = 2$ (cyan), $f = 3$ (violet), $f = 4$ (blue). T_g is defined as the temperature where $\tau_\alpha^T = 10^6$. Inset shows how the corresponding kinetic fragility κ decreases with increased self-propulsion force.

companied by a slowing down of both the translational and rotational structural relaxation process, captured by the two-step decay of the correlation functions, $Q(t)$ and $C_2(t)$ (*Supplementary Figure S2* [20]). Thus, the corresponding α-relaxation times τ_α^T and τ_α^R increase, as T or f decreases (*Supplementary Figure S3* [20]). As is usual in studies of glass forming systems, we estimate the glass transition temperature, separately for both rotational and translational relaxation, by fitting the respective α-relaxation time to a Vogel-Fulcher-Tammann (VFT) form, $\tau_\alpha = \tau_\infty \exp\left[\frac{1}{\kappa\left(\frac{T}{T_{\rm VFT}}-1\right)}\right]$, where τ_∞ is the relaxation time at large temperatures, κ is the coefficient of kinetic fragility, and $T_{\rm VFT}(f)$ is the putative glass transition temperature for an applied active force f. The resultant phase diagram in the $T-f$ plane, obtained by marking the different $T_{\rm VFT}(f)$ values, is shown in Fig. 1(b). We find that the rotational and translational degrees of freedom freeze out from the liquid at different $T_{\rm VFT}(f)$, resulting in two distinct glass phases, the translational glass (TG) and translational-rotational glass (TRG).

The phase diagram itself does not reveal any difference between approaching the glass by lowering T or f. To see differences in the active and passive systems, distinguished by their Peclet number, one needs to probe their dynamical heterogeneity. Already, the VFT fits give some hint of this: the kinetic fragility (κ) of translational glass shows a decrease with increasing activity f; see Fig. 1(c) and inset. A similar behaviour is also observed for the rotational relaxation (see *Supplementary Figure S4* [20]). Thus, the active glass becomes *stronger* or less *fragile* than a passive glass, both during translational and rotational arrest. This allows for tuning of the glassy behaviour from being fragile to strong, by tuning the magnitude of active propulsion. The decrease in fragility in an active soft supercooled liquid is consistent with some earlier numerical [5] and theoretical [23] studies. We will see later how this result is also consistent with observations in reconstituted epithelial tissues that have been reported to show glassy behaviour [24].

To explore the difference in behaviour while approaching the arrested state by either decreasing T or f, we probe the dynamics in finer detail at specific points along an iso-relaxation time ($\tau_\alpha^T = 102.85$) line (see Fig. 1(b)), which lies in the supercooled liquid regime. We measure the displacement field vectors of the centre of mass of the dumbbells, $\mathbf{d}(\mathbf{r})$, over a time τ_α^T, and construct a spatial map of corresponding streamlines, which are shown in the left panel of Fig. 2. For the passive system ($f = 0$), such a map is structureless with no large scale spatial correlation, Fig. 2(b)(left panel). On increasing Pe along the iso-τ_α^T line, one suddenly begins to observe distinct *vortex* like structures, whose size increases with increasing Pe, as seen in Fig. 2(a)(left panel). This pattern (or lack of it in the passive case) is also quantified via the coarse-grained vorticity $\omega(\mathbf{r}) = \nabla \times \mathbf{v}_\tau(\mathbf{r})$, where $\mathbf{v}_\tau(\mathbf{r}) \equiv \mathbf{d}(\mathbf{r})/\tau_\alpha^T$ [25], which are shown as underlying colormaps in the left panels of Fig. 2. Further, in the right panel of Fig. 2, we show spatial maps of the magnitude of single particle displacements during τ_α^T, to gauge the extent of dynamical heterogeneity exhibited in either situation. The active system, Fig. 2(a)(right panel), has much more spatial heterogeneity in dynamics than the passive one, Fig. 2(b)(right panel). Also, notice the anti-correlation in the vorticity and the magnitude of

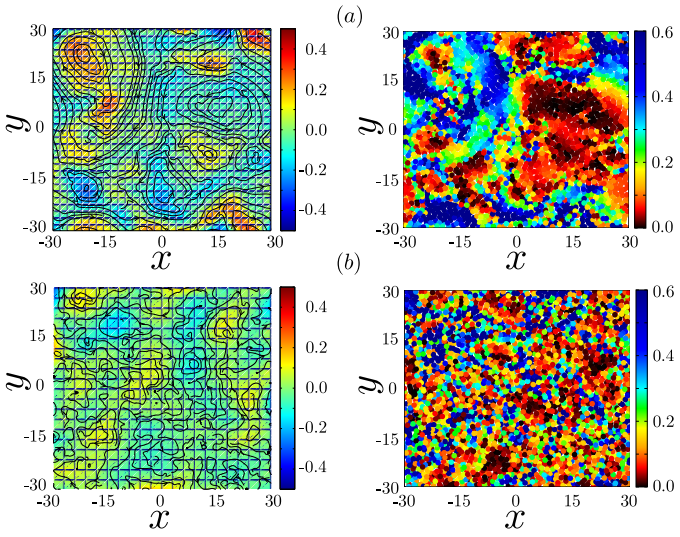

FIG. 2. (color online). (a) (*left*) Streamlines of displacement field, $\mathbf{d}(\mathbf{r})$, for the active dumbbells ($f = 10.3, T = 0$) computed over $t = \tau_\alpha^T$ showing large vortex-like structures with the underlying colormap reflecting the corresponding values of the vorticity $\omega(\mathbf{r})$. (*right*) Map showing the magnitude of displacement during $t = \tau_\alpha^T$, illustrating the extent of heterogeneous dynamics in the active glass, with blue particles being the fastest and black particles being the slowest. Note that the vorticity and particle velocities are *anti-correlated* (see text). (b) (*left*) Streamlines of displacement for passive dumbbells ($f = 0, T = 5.5$), along with corresponding vorticity colormap. (*right*) Displacement map for the passive liquid. Note the absence of any large scale structures and the resultant low vorticity.

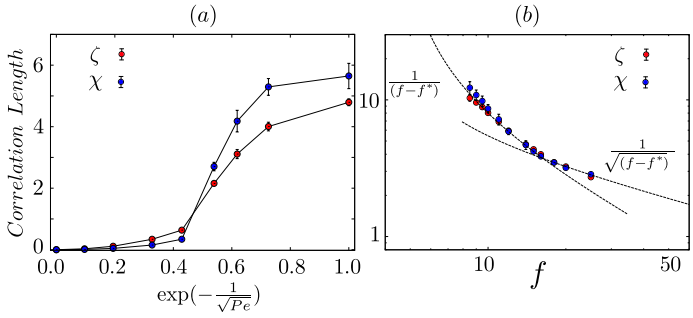

FIG. 3. (color online). (a) Correlation lengths ζ, characterizing the degree of alignment of the displacement vectors, and χ, characterizing the spatial corelation of vorticity, as a function of Pe, along the iso-τ_α^T line, show a crossover from a passive to an active supercooled liquid. To highlight the change, we subtract from the measured correlation lengths, a microscopic length associated with the size of the dumbbell. The choice of plotting against $\exp[-1/\sqrt{Pe}]$ ensures uniform spacing for the simulation data points over the range of Pe. (b) ζ and χ as a function of activity f for $T = 0$. These lengths increase and show a crossover from $1/\sqrt{f - f^*}$ dependence at large f to $1/(f - f^*)$ dependence close to the glass transition at $f^* = 4.5$.

particle displacement: regions with low (high) vorticity correspond to fast (slow) dumbbells, particles between a vortex-antivortex pair are faster, while particles in the vortex core are slower.

In order to extract correlation lengths from the spatial structures visible in such maps, we calculate the angle-averaged correlation functions of (i) the orientation of the displacement vectors of the dumbbell, $C(r) = \langle 2\cos^2 \Delta\theta(\mathbf{r}) - 1\rangle$, where $\Delta\theta(\mathbf{r})$ is the angular separation between two displacement vectors separated by distance $\mathbf{r}$ (*Supplementary Figure S5* [20]), and (ii) the vorticity, $G(r) = \langle\omega(\mathbf{0})\omega(\mathbf{r})\rangle$, evaluated over τ_α^T (*Supplementary Figure S6* [20]). The extracted correlation lengths, ζ and χ, respectively , show a crossover as we move along the iso-τ_α^T line, and distinguish the passive (low Pe) from the active (high Pe) supercooled liquids; see Fig. 3(a).

If we now move towards the dynamically arrested regime from either extreme ends, i.e. along the passive direction ($Pe = 0$) where the active forcing is absent or the athermal active direction ($Pe = \infty$) where thermal fluctuations are suppressed, we clearly observe the stark differences in the way the above-mentioned spatial correlations grow. As one goes towards the glass transition at $Pe = 0$, there is no significant change in the correlation lengths ζ and χ - which continue to remain at the scale of the dumbbell - (*Supplementary Figure S7* [20]). There is of course the usual dynamical heterogeneity associated with the emergence and growth of *fast* moving and *slow* moving domains [26] and corresponding increase in relaxation times [22, 27]. However, on approaching the glass transition from the active side, along ($Pe = \infty$), the nature of the dynamical heterogeneity is very different and is associated with swirling or vortex patterns that grow in size. The corresponding growing length scales (see Fig. 3(b)), goes as $1/\sqrt{f - f^*}$, far away from the glassy regime ($f^* = 4.5$), and crosses over to $1/(f - f^*)$, as one nears dynamical arrest.

To understand the origin of these vorticity scales, we construct a hydrodynamic description of the self-propelled dumbbells in the isotropic phase. Our simulations show that the velocity $\mathbf{v}_\tau$ is correlated with the orientation of dumbbell $\mathbf{n}$, or more precisely, $\mathbf{Q}\cdot\mathbf{f}$, where $\mathbf{Q}$ is the nematic orientation tensor describing the apolar orientation of the dumbbell and $\mathbf{f}$ is the body-attached propulsion force. This correlation increases with Peclet number along the iso-τ_α^T-line before saturating due to packing considerations (*Supplementary Figure S8* [20]). This suggests that the appropriate hydrodynamic fields are the conserved densities, orientation tensor $\mathbf{Q}$ and the dumbbell velocity $\mathbf{v}$. Note that the polarity of the dumbbells is an acquired property, a consequence of $\mathbf{Q}\cdot\mathbf{v}$. To see the generation of large swirls or vortices, it suffices to consider the dynamics of $\mathbf{Q}$ and $\mathbf{v}$ alone (*Supplementary Information* [20]). Newtons second law provides the

equation for the dumbbell velocity $\mathbf{v}$,

$$\rho\partial_t\mathbf{v} = -(\Gamma - \eta\nabla^2)\mathbf{v} + \nabla\cdot\sigma \quad (1)$$

Our use of Brownian dynamics implies that there is a frictional damping Γ, in addition to the usual viscous damping associated with the transfer of momentum arising from collisions. The last term corresponds to local forces due to a stress $\sigma = \sigma^{op} + \sigma^{act}$, written as a sum of the order parameter stress, $\sigma^{op} = \Lambda\,(\delta F/\delta\mathbf{Q}) - [\mathbf{Q}\cdot(\delta F/\delta\mathbf{Q}) - (\delta F/\delta\mathbf{Q})\cdot\mathbf{Q}]$ [21], derived from a free-energy functional, $F[\mathbf{Q}]$ for the nematic (*Supplementary Information* [20])

$$F[\mathbf{Q}] = \int d\vec{x}\left[\frac{A}{2}\mathbf{Q}^2 + \frac{C}{4}\mathbf{Q}^4 + \frac{K}{2}(\nabla\mathbf{Q})^2\right] \quad (2)$$

and $\sigma^{act} = fl\mathbf{Q}$ is the active stress [28]. The dynamics of $\mathbf{Q}$ is given by

$$D_t\mathbf{Q} = \lambda\mathbf{U} + \mathbf{Q}\cdot\mathbf{\Omega} - \mathbf{\Omega}\cdot\mathbf{Q} - \gamma^{-1}\frac{\delta F}{\delta\mathbf{Q}} \quad (3)$$

where D_t represents the convective derivative in the co-moving frame, λ is the stable-flow alignment parameter, γ is the rotational viscosity and $\mathbf{U}$ and $\mathbf{\Omega}$ are the symmetric and anti-symmetric strain-rates. Now linearising about the isotropic state with no flow, we obtain,

$$\dot{\mathbf{Q}} = \frac{\lambda}{2}\left[(\nabla\mathbf{v}) + (\nabla\mathbf{v})^T\right] - \frac{1}{\gamma}\left[A - K\nabla^2\right]\mathbf{Q} \quad (4)$$

$$\dot{\mathbf{v}} = -(\Gamma - \eta\nabla^2)\mathbf{v} + \left[\Lambda(A - K\nabla^2) + f\,l\right]\nabla\cdot\mathbf{Q} \quad (5)$$

Taking the curl of the above equations gives us the equation for the vorticity ω. Away from the glass transition, patterning is generated by balancing the active stress against the orientational elastic stress; this gives a length scale $\sqrt{\Lambda K/f\,l}$, consistent with the scaling observed in the simulations at large f (Fig. 3 and [29]). On approaching the glass transition $f = f^*$, the translational motion gets sluggish and finally arrested; it would seem that we can no longer use an active fluid description. We argue however that when $f > f^*$ we should still be able to use these equations, as long as we renormalize time by $t \to t/\tau_\alpha^T$. In this highly viscous fluid regime, the patterns are generated by balancing the active stress with the viscous stress; this gives rise to a length scale that goes as $1/(f - f^*)$ (*Supplementary Information* [20]). The crossover between these two different forms of the characteristic length with active force, occurs at propulsion force $\propto \eta^2 l/\Lambda K$.

To summarise, we study a model Brownian assembly of self-propelling soft anisotropic particles, wherein there is neither any explicit activity de-correlation time nor imposed orientational alignment, unlike many other model active systems that have been studied. We demonstrate that the active forcing makes the corresponding supercooled fluid less fragile and more importantly the heterogeneous dynamics observed in the active fluid is very different from its passive counterpart, exhibiting large-scale swirls and vortices. We further show that the correlation lengths, associated with these spatial structures, grow with decreasing active forcing and appear to diverge as the dynamics gets arrested. We rationalise the occurrence of such length scales using a continuum hydrodynamic theory of active dumbbells.

Our study of dynamical heterogeneities in active glass composed of anisotropic particles has implications for the collective cell dynamics in epithelial layers. This can be seen, by constructing a Voronoi tessellation around each dumbbell; the resulting pattern then resembles an epithelial sheet (*Supplementary Movie* [20]). One of the first studies of glassy dynamics close to the jamming transition in a reconstituted epithelial sheet [24], revealed two striking features : (i) the epithelial glass was significantly less fragile compared to a conventional hard-sphere glass and (ii) systematically reducing cell motility by treatment with titrated amounts of actin de-polymerization agents rendered the epithelial sheet more fragile. Our result on how active propulsion makes the jammed state stronger or less fragile, is entirely consistent with this. In addition, our work suggests the possibility of observing large scale swirls in situations where cellular propulsion is high and the cell-substrate adhesion is weak (*Supplementary Movie* [20]) [30].

The swirling patterns or vortex structures that we observe for dense assemblies of anisotropic particles, are reminiscent of the dynamical patterns seen in *active turbulence* exhibited by a collection of fluid of active rods [9, 10, 21]. Is the dynamical heterogeneity exhibited by the active glass a frozen memory of its active turbulent past? Our work shows unambiguously that an active glass is fundamentally distinct and not just a conventional glass with another name.

We thank A. Das, J. P. Banerjee, S. S. Ray and S. Sastry for useful discussions. RM and PJB acknowledge financial support from CSIR, India, and CD from DST, India.

* Email: rituparno@physics.iisc.ernet.in
† Email: pranab@physics.iisc.ernet.in
‡ Email: pinakic@imsc.res.in
§ Email: madan@ncbs.res.in
¶ Email: cdgupta@physics.iisc.ernet.in

[1] L. Berthier and J. Kurchan, Nat. Phys. **9**, 310 (2013).
[2] L. Berthier, Phys. Rev. Lett. **112**, 220602 (2014).
[3] R. Ni, M. A. C. Stuart and M. Dijkstra, Nat. Commun. **4**, 2704 (2013).
[4] S. Henkes, Y. Fily and M. C. Marchetti, Phys. Rev. E **84**, 040301(R) (2011).
[5] R. Mandal, P. J. Bhuyan, M. Rao and C. Dasgupta, Soft Matter **12**,6268, (2016).
[6] E. Flenner, G. Szamel and L. Berthier, Soft Matter **12**, 7136, (2016).

[7] L. F. Cugliandolo, G. Gonnella, and A. Suma, Phys. Rev. E **91**, 062124 (2015).

[8] C. Tung, J. Harder, C. Valeriani and A. Cacciuto, Soft Matter, **12**, 555 (2016).

[9] H. H. Wensink, J. Dunkel, S. Heidenreich, K. Drescher, R. E. Goldstein, H. Löwen and J. M. Yeomans, Proc. Nat. Acad. Sci. USA **109**, 14308-14313 (2012).

[10] H. H. Wensink and H. Löwen, JPCM **24**, 464130 (2012).

[11] J. T. Siebert, J. Letz, T. Speck and P. Virnau, arXiv:1611.01054 (2016).

[12] D. F. Hinz, A. Panchenko, T. Y. Kim and E. Fried, Comp. Phys. Comm. **196**, 45 (2015).

[13] J. A. Park *et al.*, Nat. Mater. **14**, 1040-1048 (2015).

[14] D. Bi, J. H. Lopez, J. M. Schwarz, and M. L. Manning, Nat. Phys. **11**, 1074 (2015).

[15] N. Kumar, H. Soni, S. Ramaswamy and A. K. Sood, Nat. Commun. **5**, 4688 (2014).

[16] W. Kob and H. C. Andersen, Phys. Rev. Lett. **73**, 1376 (1994).

[17] S. H. Chong, A. J. Moreno, F. Sciortino and W. Kob, Phys. Rev. Lett. **94**, 215701 (2005).

[18] A.J. Moreno, S.H. Chong, W. Kob and F. Sciortino, J. Chem. Phys. **123**, 204505 (2005).

[19] S. H. Chong and W. Kob, Phys. Rev. Lett. **102**, 025702 (2009).

[20] See Supplementary Information.

[21] L. Giomi, Phys. Rev. X **5**, 031003 (2015).

[22] S. Karmakar, C. Dasgupta and S. Sastry, Proc. Nat. Acad. Sci. USA **106**, 3675 (2009).

[23] S.K. Nandi, arXiv:1605.06073 (2016).

[24] E. H. Zhou *et al.*, Proc. Nat. Acad. Sci. USA **106**, 10632 (2009).

[25] This differs from the usual definition based on instantaneous velocities and reflects the fact that dynamics in the supercooled regime manifests only over α-relaxation times.

[26] L. Berthier and G. Biroli, Rev. Mod. Phys. **83**, 587 (2011).

[27] S. Karmakar, C. Dasgupta and S. Sastry, Annu. Rev. Condens. Matter Phys. **5**, 255-284 (2014).

[28] M. C. Marchetti *et al.*, Rev. Mod. Phys. **84**, 040301 (2014).

[29] E. J. Hemingway, P. Mishra, M. C. Marchetti and S. M. Fielding, Soft Matter **12**, 7943-7952 (2016).

[30] T. E. Angelini *et al.*, Proc. Nat. Acad. Sci. USA **10**, 1073 (2011).

Glassy swirls of active dumbbells - Supplementary Information

Rituparno Mandal,[1,*] Pranab Jyoti Bhuyan,[1,†] Pinaki Chaudhuri,[2,‡] Madan Rao,[3,§] and Chandan Dasgupta[1,¶]

[1] *Centre for Condensed Matter Theory, Department of Physics, Indian Institute of Science, Bangalore 560012, India*
[2] *The Institute of Mathematical Sciences, Chennai 600113, India*
[3] *Simons Centre for the Study of Living Machines, National Centre for Biological Sciences (TIFR), Bangalore 560065, India*

arXiv:1703.05484v1 [cond-mat.soft] 16 Mar 2017

* Email: rituparno@physics.iisc.ernet.in
† Email: pranab@physics.iisc.ernet.in
‡ Email: pinakic@imsc.res.in
§ Email: madan@ncbs.res.in
¶ Email: cdgupta@physics.iisc.ernet.in

S1. MODEL AND SIMULATION DETAILS

For our study, we perform Brownian dynamics simulation of a two-dimensional binary dumbbell mixture. Each dumbbell consists of two spherical monomers of the same type (either A or B) connected via a spring with a stiffness of $k = 200$; a schematic of the dumbbell is illustrated in the inset of *Fig.1* in the main paper. This value of spring constant makes the dumbbells fairly rigid with an equilibrium length $l = \sigma_{\alpha\alpha}/2$ (where $\alpha \in A, B$) between the centers of the two monomers of each dumbbell [1–3]. The mixture consists of 50:50 A-A and B-B dumbbells, which leads to amorphous structures. The equation of motion for each monomer can be written as,

$$\dot{\mathbf{r}}_i = \frac{1}{\gamma}\left[\sum_{j\in\mathbb{NN}} \mathbf{f}_{ij} - k(\mathbf{r}_i - \mathbf{r}_{i'} - l\mathbf{n}_i) + f\mathbf{n}_i\right] + \boldsymbol{\eta}_i \tag{S1}$$

where γ is the friction coefficient, $\mathbf{f}_{ij}$ is the interaction force between the i-th and the j-th monomer, i and i' denote the two monomers of the same dumbbell, $\mathbf{n}_i$ is the unit vector in a pre-specified direction along the long axis of the dumbbell associated with the i-th particle, f is the strength of the propulsion force and $\boldsymbol{\eta}_i$ is the thermal noise which satisfies fluctuation-dissipation relation of the form $\langle \eta_i^\alpha(t)\eta_i^\beta(t')\rangle = 2D\delta_{\alpha\beta}\delta(|t-t'|)$ (where $\alpha, \beta \in x, y$) with $\langle \boldsymbol{\eta}_i(t)\rangle = 0$, $D = \frac{k_B T}{\gamma}$; T is the temperature of the heat bath. The interaction force ($\mathbf{f}_{ij}$) between the monomers is modelled via the Lennard-Jones pair potential,

$$V_{ij}(r) = 4\epsilon_{\alpha\beta}\left[\left(\frac{\sigma_{\alpha\beta}}{r_{ij}}\right)^{12} - \left(\frac{\sigma_{\alpha\beta}}{r_{ij}}\right)^{6}\right], \tag{S2}$$

where r_{ij} is the distance between the i-th and the j-th particle *i.e.* $r_{ij} = |\mathbf{r}_i - \mathbf{r}_j|$ where α, β represent either A-type or B-type particles. In our simulation we have chosen the values of $\sigma_{\alpha\beta}$ and $\epsilon_{\alpha\beta}$ to be: $\sigma_{AB} = 0.8\sigma_{AA}$, $\sigma_{BB} = 0.88\sigma_{AA}$, $\epsilon_{AB} = 1.5\epsilon_{AA}$, $\epsilon_{BB} = 0.5\epsilon_{AA}$. The potential has been truncated at $r^c_{\alpha\beta} = 2.5\sigma_{\alpha\beta}$ and the potential has been shifted accordingly such that both the potential and the force are continuous at the cut-off. The unit of length and energy in our simulation are set by $\sigma_{AA} = 1$ and $\epsilon_{AA} = 1$ and the study is done for an overall number density of $\rho = 1.6$.

In our model, *activity* is introduced via a self-propulsion force of magnitude f which acts on each monomer, of each dumbbell, in a pre-specified direction along the corresponding dumbbell axis. Therefore, although each dumbbell consists of two identical beads, there exists a polar vector attached to each dumbbell which breaks the head-to-tail symmetry, via the corresponding direction of the self-propulsion force. The control parameter for activity f is also the measure of the extent of non-equilibrium behaviour introduced in the system.

For such a system of particles, we carry out Brownian dynamics simulation, using the Euler algorithm. The *temperature* T for both passive and active system is determined by the heat bath to which the system is coupled.

The number of integration step for the simulation is between 10^8 and 10^9 depending on the parameters with a time-step of integration $dt = 10^{-3}$. We have compared our Brownian dynamics results to those of Newtonian dynamics simulations and observed that the long time dynamics is quantitatively similar for the parameter ranges we have studied, as expected. For each parameter set, the results presented here have been averaged over 16-32 independent trajectories.

S2. HYDRODYNAMIC CALCULATION

We now construct a hydrodynamic description of the self-propelled dumbbells in terms of their conserved densities, orientation tensor $\mathbf{Q}$ and the dumbbell velocity $\mathbf{v}$. The fact that it is a two-component system just goes towards forming a translational and orientational glass - it is not relevant to the generation of the large swirls or vortices. We will therefore treat it as a one-component system with a single conserved density field ρ, whose dynamics is given by,

$$\partial_t \rho + \nabla\cdot(\rho\mathbf{v}) = 0 \tag{S3}$$

Newton's second law provides the equation for the dumbbell velocity $\mathbf{v}$,

$$\rho\partial_t\mathbf{v} = -(\Gamma - \eta\nabla^2)\mathbf{v} - \zeta_c\nabla\rho + \nabla\cdot\sigma. \tag{S4}$$

Γ represents frictional damping and η is the viscosity associated with the transfer of momentum arising from collisions. The second term on the right, may be thought of as a pressure term arising from density inhomogeneities; ζ_c is therefore

a compressibility. The last term on the right is the contribution to the force coming from the total deviatoric stress σ. In the high density phase at the onset of glassy behaviour one might choose to ignore spatial inhomogeneities of the density. There are however non-trivial temporal correlations of the density, but since we only want to extract the swirling behaviour, we ignore this. This leads to Eq. (1) in the main text. The total deviatoric stress $\sigma = \sigma^{op} + \sigma^{act}$, is a sum of the order parameter stress, $\sigma^{op} = \Lambda\,(\delta F/\delta \mathbf{Q}) - [\mathbf{Q}\cdot(\delta F/\delta\mathbf{Q}) - (\delta F/\delta\mathbf{Q})\cdot\mathbf{Q}]$ [4], derived from a free-energy functional for the nematic,

$$F[\mathbf{Q}] = \int d\vec{x}\Big[\frac{A}{2}\mathbf{Q}^2 + \frac{C}{4}\mathbf{Q}^4 + \frac{K}{2}(\nabla\mathbf{Q})^2\Big], \tag{S5}$$

and the active stress $\sigma^{act} = fl\mathbf{Q}$ [5]. From this we get,

$$\delta F/\delta\mathbf{Q} = \Big[(A + \frac{C}{2}S^2)\mathbf{Q} - K\nabla^2\mathbf{Q}\Big] \tag{S6}$$

where S is the magnitude of the nematic order parameter present in the system and $S^2 = 2\mathrm{Tr}(\mathbf{Q}^2)$. We also have the time evolution equation for $\mathbf{Q}$,

$$D_t\mathbf{Q} = \lambda\mathbf{U} + \mathbf{Q}\cdot\mathbf{\Omega} - \mathbf{\Omega}\cdot\mathbf{Q} - \gamma^{-1}\frac{\delta F}{\delta\mathbf{Q}} \tag{S7}$$

where D_t represents the convective derivative in the comoving frame, λ is the stable-flow alignment parameter, γ is the rotational viscosity and $\mathbf{U}$ and $\mathbf{\Omega}$ are the symmetric and anti-symmetric strain-rates; $\mathbf{U} = \frac{1}{2}\left[(\nabla\mathbf{v}) + (\nabla\mathbf{v})^T\right]$ and $\mathbf{\Omega} = \frac{1}{2}\left[(\nabla\mathbf{v}) - (\nabla\mathbf{v})^T\right]$.

Upon linearising about the isotropic state with no flow, we get equations Eqs. 4, 5 in the main text.

Discussion on length scales : The lengths scales associated with the spatial patterning of the vortex flows can be obtained using dimensional analysis by balancing the relevant contributions to the stress appearing in Eq. 5 in the main text.

Away from the glass transition, patterning is generated by balancing the active stress ($fl\mathbf{Q}$) against the orientational elastic stress ($\Lambda K\nabla^2\mathbf{Q}$). This gives a length scale $\sqrt{\Lambda K/fl}$, consistent with the scaling observed in our simulations at large f.

On approaching the glass transition $f = f^*$, the translational motion gets sluggish and finally arrested. As long as $f > f^*$, the system is still an active *fluid*, and flows over a time scale τ_α^T. We thus argue that we should still be able to use the active fluid equations, Eq. 4, 5, as long as we renormalize time by $t \to t/\tau_\alpha^T$. In this highly viscous fluid regime, the patterns are generated by balancing the active stress ($fl\mathbf{Q}$) with the viscous stress ($\eta\nabla\mathbf{v}$). Note that the velocity scale that appears in the balance above is the coarse-grained velocity $\mathbf{v}_\tau$. From our simulations, the typical magnitude of $\mathbf{v}_\tau$ is of order l, in units of this scaled time. Using this we get the length scale for the spatial patterning of the velocity to go as $\eta/(f - f^*)$, as long as f is greater than, but close to, f^*.

The crossover between these two behaviours occurs at a propulsion force $\propto \eta^2\, l/\Lambda K$.

[1] S. H. Chong, A. J. Moreno, F. J. Sciortino and W. Kob, Phys. Rev. Lett. **94**, 215701 (2005).
[2] D. F Hinz, A. Panchenko, T-Y Kim and E. Fried, Comp. Phys. Comm. **196**, 45 (2015).
[3] L. F. Cugliandolo, G. Gonnella and A. Suma, Phys. Rev. E **91**, 062124 (2015).
[4] L. Giomi, Phys. Rev. X **5**, 031003 (2015).
[5] M. C. Marchetti *et al.*, Rev. Mod. Phys. **84**, 040301 (2014).

S3. SUPPLEMENTARY FIGURES

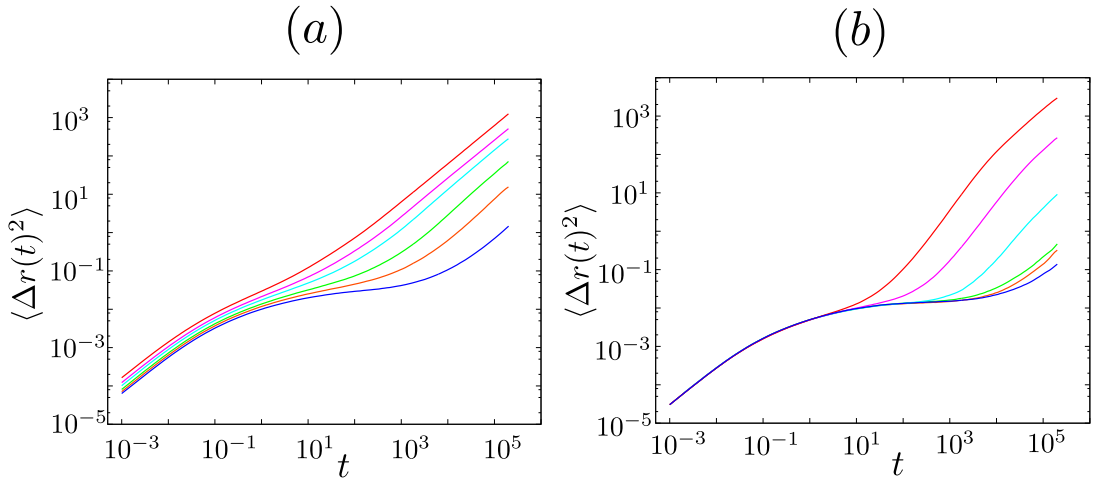

FIG. S1. (color online). Mean squared displacement ($\langle \Delta r(t)^2 \rangle$) as function of t - (a) for propulsion force f=2.0 for different temperatures T=3 (blue), 3.5 (orange),4 (green), 5 (cyan), 6 (magenta), 8 (red) and (b) for temperature T=1.5 for different propulsion forces f=3 (blue), 3.5 (orange),4 (green), 5 (cyan), 6 (magenta), 8 (red).

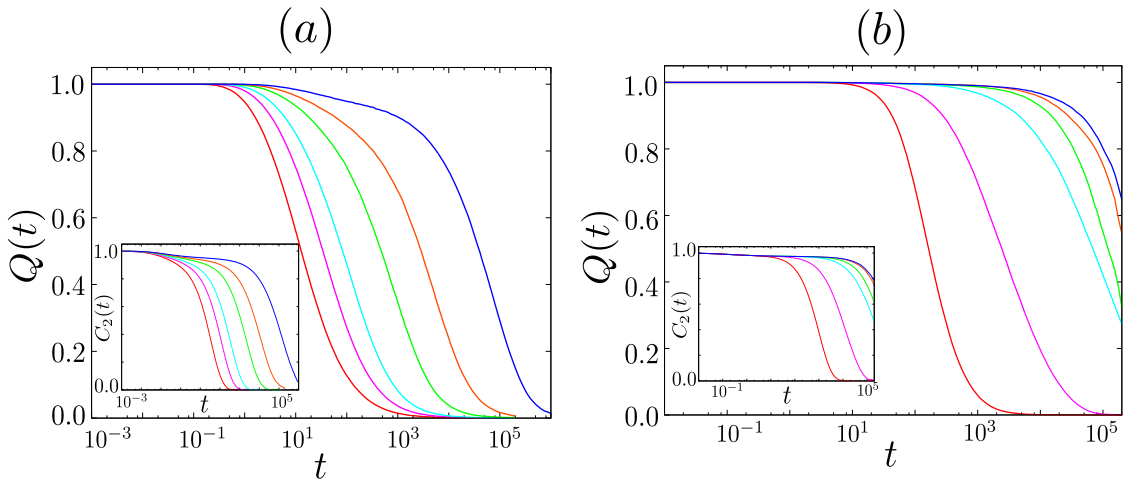

FIG. S2. (color online).(a) Overlap function, $Q(t)$, measured for propulsion force f=2 at different temperatures T=3 (blue), 3.5(orange), 4 (green), 5 (cyan), 6 (magenta), 8 (red) and (b) for temperature T=1.5 for different propulsion forces f=3 (blue), 3.5 (orange),4 (green), 5 (cyan), 6 (magenta), 8 (red). Inset shows rotational time correlation function, $C_2(t)$, and its behaviour for the same set of parameters in both the cases.

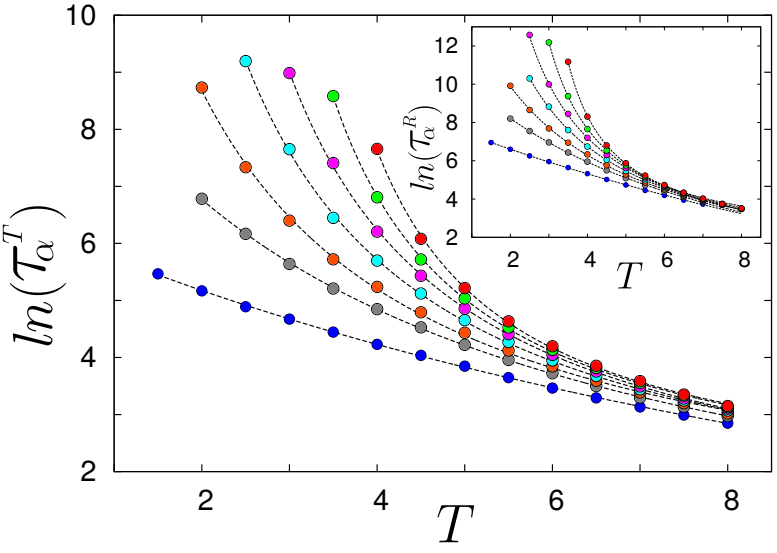

FIG. S3. (color online). Translational α-relaxation time scale (in filled circles) as a function of temperature (T) for different values of self-propulsion force (f= 0 (red), 2 (green), 3 (magenta), 4 (cyan), 5 (orange), 6 (dark grey), 8 (blue)). The black dotted lines represent the fiitting of the data sets for each f to the VFT form. Inset shows rotational α-relaxation time scale (in filled circles) as a function of temperature (T) for the same values of self-propulsion force (f).

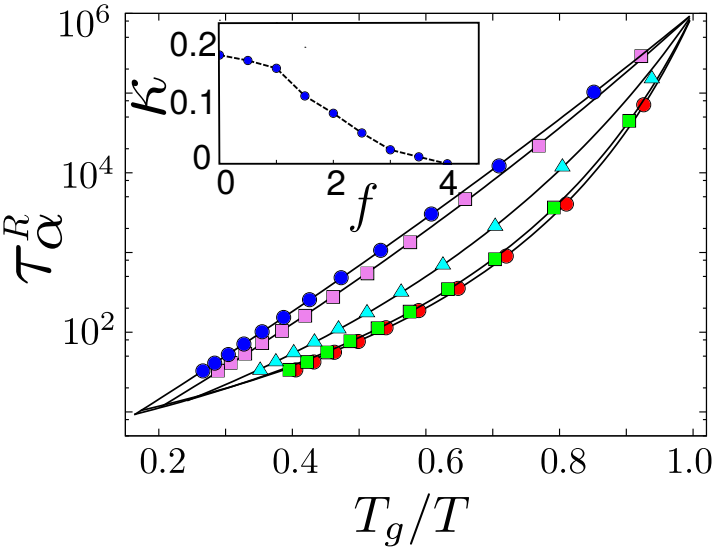

FIG. S4. (color online). Variation of rotational relaxation times τ_α^R versus scaled temperature (T_g/T) with changing active force : $f = 0$ (red), $f = 1$ (green), $f = 2$ (cyan), $f = 3$ (violet), $f = 3.5$ (blue). T_g is defined as the temperature where $\tau_\alpha^R = 10^6$. Inset shows how the corresponding kinetic fragility κ decreases with increased self-propulsion force.

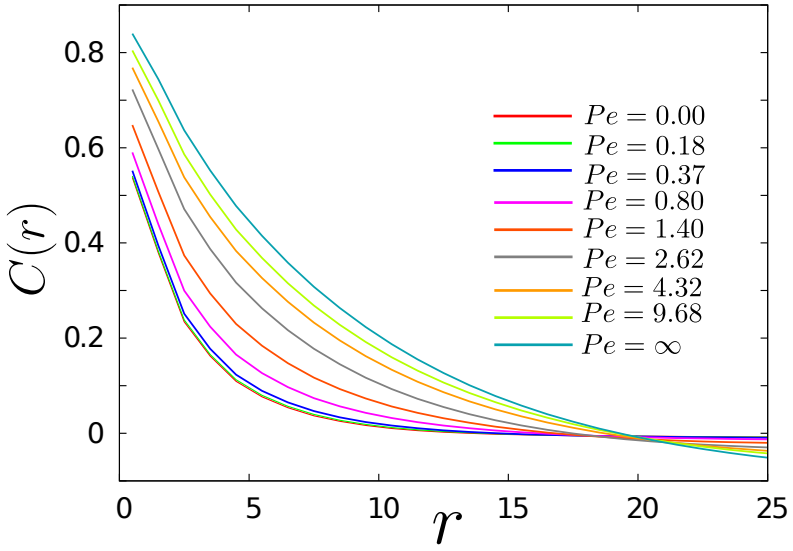

FIG. S5. (color online). Spatial correlation function of the orientation of the displacement vectors of the center of mass of the dumbbells, $C(r) = \frac{1}{2\pi}\int \langle 2\cos^2 \Delta\theta(\mathbf{r}) - 1\rangle d\phi$, where $\Delta\theta(\mathbf{r})$ is the angular separation between two displacement vectors separated by distance $\mathbf{r}$. The simulation points are chosen along an iso-τ_α^T line on the $(T-f)$ phase diagram. The correlation length ζ is extracted using the condition $C(\zeta) = 1/e$.

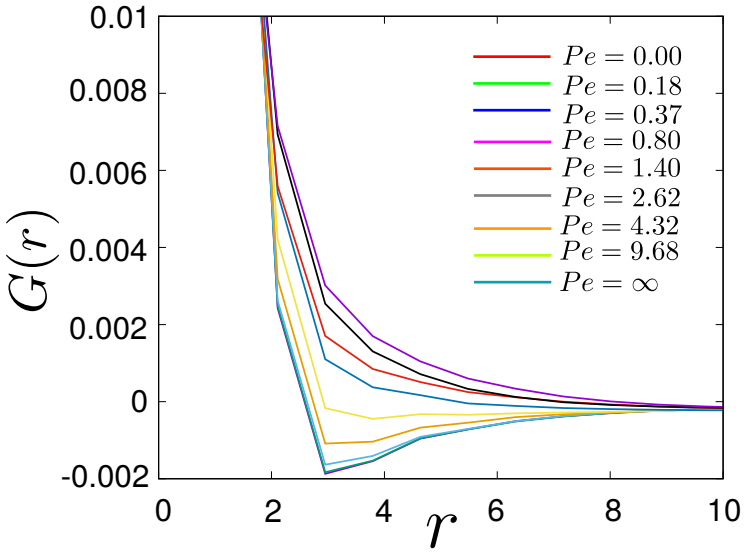

FIG. S6. (color online). Spatial correlation of the vorticity field of the coarse grained velocity vectors $G(r) = \frac{1}{2\pi}\int \langle \omega(\mathbf{0})\omega(\mathbf{r})\rangle d\phi$ over a time scale of τ_α^T. The simulation points are chosen along an iso-τ_α^T line on the $(T-f)$ phase diagram. The correlation length χ is extracted using the condition $G(\chi) = 0$.

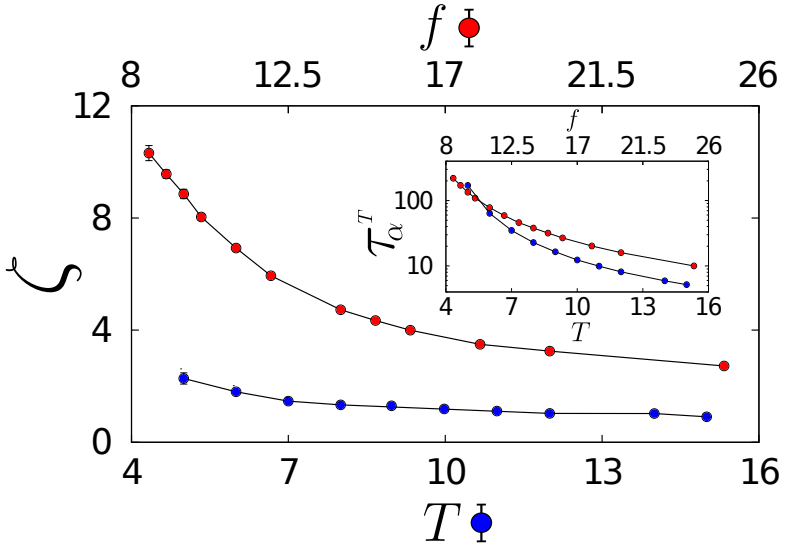

FIG. S7. (color online). Length scale (ζ) associated with spatial correlation of the direction of the displacement vectors for the dumbbell system at $f = 0$ for different T (blue) and at $T = 0$ for different f (red), *i.e.*, when we approach the glass boundary along two different axes. The correlation length scale does not show any significant change if the glass transition is approached by reducing temperature but shows an increase as the system approaches a glass transition by reducing the activity. Inset shows relaxation time scale (τ_α^T) for similar set of simulation points at $f = 0$ for different T and at $T = 0$ for different f.

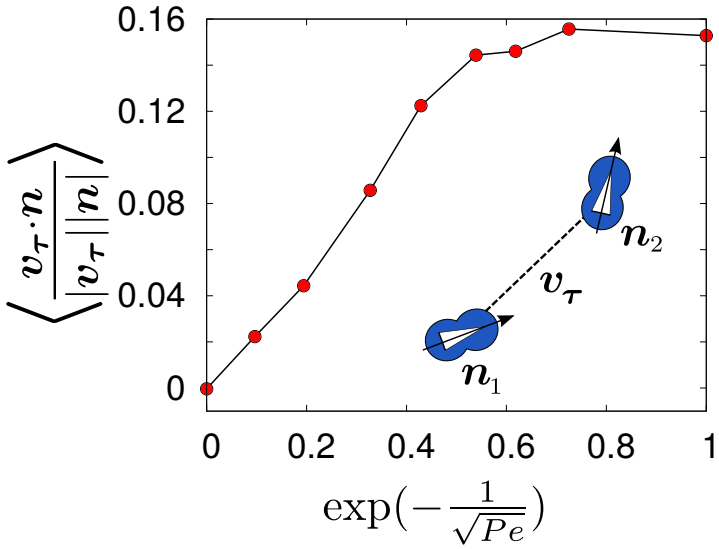

FIG. S8. (color online). Average of the normalized dot product of the coarse grained velocity ($\mathbf{v}_\tau$) of each dumbbell and its average orientation vector ($\mathbf{n} = \frac{\mathbf{n1}+\mathbf{n2}}{2}$) over the α-relaxation time (τ_α^T) as we move through different points on the iso-τ_α^T line from passive to active supercooled liquid region. For few initial points the correlation between displacement and orientation increases and then it saturates as maximum coupling between these two is reached, which is limited by the packing of the dumbbells.

S4. SUPPLEMENTARY MOVIES

The movies illustrate the time evolution of Voronoi tessellations, constructed from the dumbbell configurations. Each Voronoi cell is associated with the center of mass of each dumbbell. The movies are shown for two points on the iso-τ_α line explored in our work, viz. (i) $T = 5.4678, f = 1$ (weakly active supercooled liquid – *movie1.avi*) and (ii) $T = 0, f = 10.27$ (strongly active supercooled liquid – *movie2.avi*). For the movies, we focus on approximately one quadrant of the whole simulation box, in order to properly visualize the topological changes that happen within the system. In *movie1.avi* we mainly observe thermal vibrations with occasional uncorrelated rearrangements of cells, while in *movie2.avi* we observe large scale collective rearrangements of cells. As stated in the main text, this is likely to be relevant for collective cell motion in epithelial tissues.